Article

High carbon dioxide emissions from Australian estuaries driven by geomorphology and climate

Jacob Z.-Q. Yeo [1] ✉, Judith A. Rosentreter [1], Joanne M. Oakes [1], Kai G. Schulz [1] & Bradley D. Eyre [1]

Estuaries play an important role in connecting the global carbon cycle across the land-to-ocean continuum, but little is known about Australia's contribution to global CO_2 emissions. Here we present an Australia-wide assessment, based on CO_2 concentrations for 47 estuaries upscaled to 971 assessed Australian estuaries. We estimate total mean (±SE) estuary CO_2 emissions of 8.67 ± 0.54 Tg CO_2-C yr^{-1}, with tidal systems, lagoons, and small deltas contributing 94.4%, 3.1%, and 2.5%, respectively. Although higher disturbance increased water-air CO_2 fluxes, its effect on total Australian estuarine CO_2 emissions was small due to the large surface areas of low and moderately disturbed tidal systems. Mean water-air CO_2 fluxes from Australian small deltas and tidal systems were higher than from global estuaries because of the dominance of macrotidal sub-tropical and tropical systems in Australia, which have higher emissions due to lateral inputs. We suggest that global estuarine CO_2 emissions should be upscaled based on geomorphology, but should also consider land-use disturbance, and climate.

Estuaries play an important role connecting the carbon cycle across the land-to-ocean aquatic continuum, processing large amounts of allochthonous and autochthonous carbon[1]. This is despite estuaries constituting only a small fraction of the world's surface (0.2%)[2] compared to continental shelf seas (5%)[3] and the open ocean (64%)[4]. Carbon from upstream rivers and associated coastal wetlands entering estuaries is either buried (and potentially stored long-term), emitted to the atmosphere in the form of greenhouse gases, or exported to the ocean[5,6]. Estuarine CO_2 emissions are estimated to equate to the size of the CO_2 sink in shelf seas (0.268 ± 0.225 Pg C yr^{-1}), or 19% of the CO_2 sequestration in the open ocean[7], but early estimates were mostly based on studies in the northern hemisphere (e.g. refs. 5,6,8,9). CO_2 emissions from estuaries can differ between estuary geomorphic types[10,11], but the mechanisms by which geomorphology affects estuarine CO_2 emissions in Australia have not been determined. There is also limited knowledge of how disturbance impacts CO_2 emissions and how different geomorphic estuary types modify any disturbance effect.

Low to high disturbance and land-use changes in the upper catchment have the potential to alter the quantity and quality of carbon delivered to estuaries[5,12], and hence the associated estuary CO_2 emissions[12,13]. Dissolved inorganic carbon (DIC)[14], dissolved organic carbon (DOC)[15], and particulate organic carbon (POC)[16] inputs typically increase in impacted estuaries and tend to be associated with increased CO_2 emissions[7,17,18]. However, the effect of land-use on CO_2 emissions from estuaries can vary[12,19]. For instance, moderately and highly disturbed estuaries in Australia have been reported to emit more CO_2 per unit area (37 ± 10 mmol CO_2-C m^{-2} d^{-1}) than less disturbed estuaries (6.3 ± 4 mmol CO_2-C m^{-2} d^{-1})[12], whereas very small coastal estuaries with high land-use changes (>90% of catchment modified) had lower CO_2 emissions than estuaries with low land-use changes (~21% of catchment modified)[15]. Moreover, changes in land-use along an estuarine gradient can influence nutrient cycling (e.g., decomposition) and change the quantity and quality (labile or refractory) of organic matter inputs[20–22], resulting in increases or decreases

¹Centre for Coastal Biogeochemistry, Faculty of Science and Engineering, Southern Cross University, PO Box 157, East Lismore, NSW 2480, Australia.
✉e-mail: jacob.yeo@scu.edu.au

in CO_2 emissions between riverine-upstream, mid-estuary, and near-marine regions[23,24].

Estuaries of different geomorphology are the result of varying influences of river discharge, tidal amplitude, and wave energy, which determine estuarine hydrological characteristics such as water depth, current velocity, and water residence times[2,25,26]. In turn, water depth and current velocity influence the gas transfer velocity (k) which controls the rate of CO_2 emission from the water into the atmosphere[27–29]. Water residence times control CO_2 emissions in estuaries by determining the direction and intensity of estuarine water-air CO_2 fluxes[2,7], because long water residence times allow for more carbon decomposition, resulting in increased DIC that can be emitted as CO_2[7,28,30]. Shorter water residence times accelerate DOC export to the ocean, resulting in lower CO_2 emissions[17,18]. Stratification of the water column can also influence CO_2 emissions[31,32]. Photosynthetic CO_2 uptake occurs in the surface layer, whereas CO_2 respired in the bottom waters is isolated from atmospheric exchange at the surface[32–34], resulting in an overall increase in CO_2 partial pressure ($p$$CO_2$) but unaffected water-air CO_2 flux rates[32,34]. Stratification occurs in estuaries with weak tidal forcing, which leads to the separation of water layers of different densities (i.e. salinities)[31,35] or temperatures (thermohaline stratification)[32–34]. In estuaries with stronger tidal influence, tidal pumping can also increase CO_2 emissions through the lateral import of DIC and DOC from coastal wetlands to the estuary[36,37]. Tidal pumping can be a significant driver of CO_2 emissions, with groundwater-derived export accounting for 93% to 99% of DIC and 89% to 92% of DOC exported from mangroves into tidal creeks[36]. In very large river systems[2] such as the Amazon River[38] in Brazil and the Yangtze[39] River in China, riverine transport from the estuary to the ocean can result in extensive estuarine plumes that can act as either a source or a sink of CO_2. However, such systems do not exist in Australia. A recent global analysis showed that fjords predominantly act as CO_2 sinks, while tidal systems and deltas emit more CO_2 than lagoons[11].

Australia makes a significant contribution to the total number and surface area of estuaries globally. Australia's coastline of 36,700 km includes 971 estuaries[40], accounting for 1.82% of the total number of estuaries globally[41] and 2.35% of global estuarine surface area[2]. More importantly, the majority of Australia's estuaries (70.6%) are classified as low or moderately disturbed[40], contrasting with predominantly disturbed estuaries in Europe and the United States where the majority of estuarine CO_2 emissions have been measured[9,10]. This reflects Australia's population density of only 3.3 persons km^{-2}[42], the 3rd lowest in the world. Despite Australia's contribution to global estuary number and surface area, CO_2 emissions have been measured in only a few Australian estuaries (e.g. refs. 12,23,43,), and there are no estimates of total CO_2 emissions from Australian estuaries. In this study, we (1) calculated CO_2 emissions from $p$$CO_2$ measurements from 36 estuaries in different climate zones in Australia and combined these CO_2 emission estimates with previously published CO_2 emissions from 11 other Australian estuaries[12,30] (total of 47 estuaries), and (2) assessed the interaction effects of anthropogenic disturbance and geomorphology on CO_2 emissions for these 47 estuaries. Based on disturbance and geomorphology classifications of Australian estuaries, we then scaled up CO_2 emissions from the 47 estuaries to all 971 assessed estuaries to better constrain Australia's contribution to global estuarine CO_2 emissions. We hypothesised that estuarine geomorphic type and
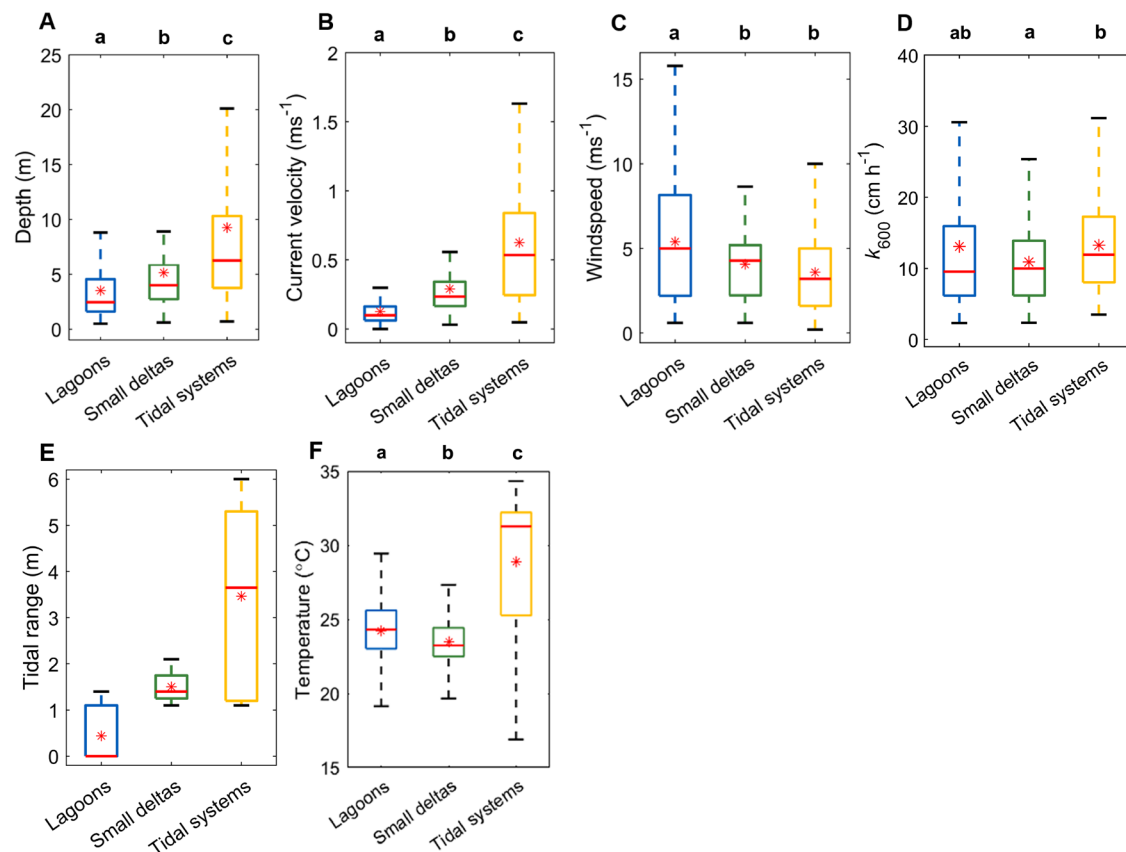
Fig. 1 | Physical parameters in the three estuary types. Median (red line), mean (red asterisk), 1st and 3rd interquartile ranges (box caps), minimum, and maximum values (whiskers) of (**A**) water depth, (**B**) current velocity, (**C**) wind speed, (**D**) mean gas transfer velocity normalised to Schmidt no. 600 (k_{600}) calculated from the five parameterisations (Table 2), (**E**) tidal range, and (**F**) temperature in the lagoons (blue, n: **A** = 92, **B** = 101, **C** = 88, **D** and **F** = 3789, and **E** = 21), small deltas (green, n: **A** = 75, **B** = 67, **C** = 79, **D** = 3362, **E** = 12, and **F** = 3622), and tidal systems (yellow, n: **A** = 121, **B** = 112, **C** = 126, **D** = 5207, **E** = 14, and **F** = 5720). Outliers were omitted from the graphs. Letters above figures denote statistical differences among estuary types, with letters that are the same indicating no significant difference (PERMANOVA, two-tailed, and at 95% confidence interval). Source data are provided as a Source Data file.
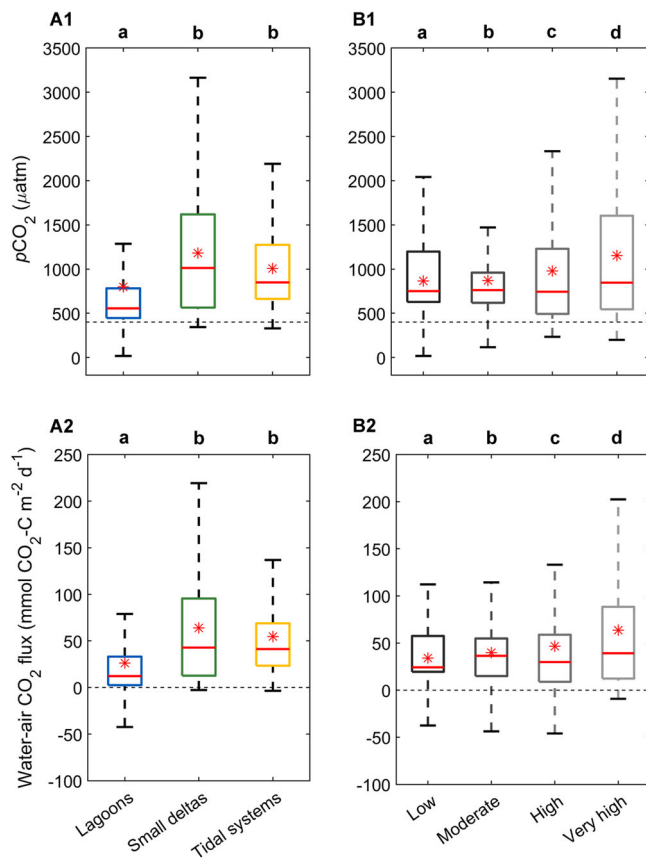
Fig. 2 | CO$_2$ partial pressure (pCO$_2$) and water-air CO$_2$ flux in estuary types and disturbance groups. Median (red line), mean (red asterisk), 1st and 3rd inter-quartile ranges (box caps), minimum and maximum values (whiskers) of pCO$_2$ and water-air CO$_2$ flux at per-minute resolution in the (**A**) lagoons (blue, $n = 3789$), small deltas (green, $n = 3622$), and tidal systems (yellow, $n = 5720$); and (**B**) low (black, $n = 1796$), moderate (dark grey, $n = 3189$), high (grey, $n = 3677$), and very high (light grey, $n = 4469$) disturbance groups. Outliers were omitted from the figures. Dotted line along the x-axis represents atmospheric pCO$_2$ and water-air flux CO$_2$ equilibrium. Letters above figures denote statistical differences among estuary types, with letters that are the same indicating no significant difference (PERMANOVA, two-tailed, and at 95% confidence interval). Source data are provided in the Source Data file.

disturbance level (including land-use change) would significantly impact estuarine water column pCO$_2$ and CO$_2$ emissions, and that there would be an interaction between geomorphic type, disturbance level, and CO$_2$ emissions. We further hypothesised that relative CO$_2$ emissions from Australian estuaries would be lower than global estuary CO$_2$ emissions because of generally lower disturbance found in estuaries in Australia.

Results

Physical differences between estuary types

Mean (min-max) tidal range was highest in tidal systems ($n = 14$) (3.7 m (1.1–6.0 m)), moderate in small deltas ($n = 12$) (1.5 m (1.1–2.1 m)), and generally lower in lagoons ($n = 21$) (0.6 m (0–1.4 m)) (Fig. 1E). Water depth ($n = 92$, 75, and 121, respectively) (Fig. 1A) and current velocity ($n = 101$, 67, and 112, respectively) (Fig. 1B) significantly increased ($p = 0.001$) from lagoons to small deltas to tidal systems. Wind speed was significantly higher in lagoons ($n = 88$) than in small deltas ($n = 79$) ($p = 0.004$) and tidal systems ($n = 126$) ($p = 0.001$), but was similar between small deltas and tidal systems ($p = 0.137$) (Fig. 1C). The mean gas transfer velocity normalised to the Schmidt number of 600 (k_{600}), was highest in tidal systems and significantly lower in small deltas

($p = 0.001$). Although lagoons had the lowest k_{600} ($n = 751$), it was not significantly different from small deltas ($n = 667$) and tidal systems ($n = 1036$) (negative t-values) (Fig. 1D and Supplementary Fig. 1). Tidal range significantly increased from the lowest in lagoons ($n = 21$) to the highest in tidal systems ($n = 14$, small deltas: $n = 12$) ($p = 0.001$) (Fig. 1E). Temperature differed significantly between estuary types (lagoons: $n = 751$) ($p = 0.001$) with the lowest mean temperature in small deltas ($n = 719$) and the highest mean temperature in tidal systems ($n = 1138$) (Fig. 1F and Supplementary Table 3). Across all estuary types, except tidal systems, and within estuary types, temperature did not significantly correlate with pCO$_2$ and water-air CO$_2$ flux. In tidal systems, there was a significant increase in water-air CO$_2$ flux with temperature ($r = 0.254$, $p = 0.01$).

Estuary pCO$_2$ and water-air CO$_2$ fluxes

The majority of the estuaries studied were a source of CO$_2$ to the atmosphere (Fig. 2A). Mean ($\pm$SE) pCO$_2$ and water-air CO$_2$ fluxes were 799 ± 13 µatm and 26.4 ± 0.9 mmol CO$_2$-C m^{-2} d^{-1} in lagoons ($n = 751$), 1181 ± 12 µatm and 63.9 ± 1.1 mmol CO$_2$-C m^{-2} d^{-1} in small deltas ($n = 719$), and 1007 ± 6 µatm and 54.8 ± 0.8 mmol CO$_2$-C m^{-2} d^{-1} in tidal systems ($n = 1138$) (Table 1). Six small deltas and three tidal systems had small sections that were weak CO$_2$ sinks (>-3.5 mmol CO$_2$-C m^{-2} d^{-1}). Four lagoons were overall CO$_2$ sinks, whereas 14 lagoons had sections that were strong CO$_2$ sinks (up to -64.7 mmol CO$_2$-C m^{-2} d^{-1}). Although pCO$_2$ and water-air CO$_2$ fluxes in the lagoons had the largest range, pCO$_2$ and water-air CO$_2$ fluxes were significantly lower than in small deltas and tidal systems ($p = 0.001$), with lower means and medians (Fig. 2A). pCO$_2$ ($p = 0.693$) and water-air CO$_2$ fluxes ($p = 0.064$) in small deltas were not significantly different to those in tidal systems (Fig. 2A).

Disturbance effects on estuary CO$_2$

pCO$_2$ and water-air CO$_2$ fluxes significantly increased with greater disturbance in Australian estuaries (low to very high disturbance, n = 356, 633, 731, and 888, respectively) (Fig. 2B). For example, mean water-air CO$_2$ fluxes across all estuary types increased from 34.1 ± 0.8 mmol CO$_2$-C m^{-2} d^{-1} in the low disturbance systems to 63.8 ± 1.2 mmol CO$_2$-C m^{-2} d^{-1} in the very high disturbance systems (Table 1). However, the effect of disturbance on pCO$_2$ and water-air CO$_2$ fluxes was estuary type specific (Fig. 3). In the lagoons, pCO$_2$ in the low disturbance systems ($n = 41$) was below atmospheric equilibrium (Fig. 3A1), with CO$_2$ influx from the atmosphere into the estuarine waters (range: 17 to 436 µatm, -46.2 to 4 mmol CO$_2$-C m^{-2} d^{-1}; Figure 3A2). pCO$_2$ increased significantly in higher disturbance lagoons ($p = 0.001$), except between highly and very highly disturbed lagoons ($p = 0.934$) (moderate to very high disturbance, n = 161, 261, and 288, respectively). Similarly, water-air CO$_2$ flux in lagoons increased significantly with higher disturbance ($p = 0.001$), but only from low to high disturbance, and was significantly lower in very high disturbance lagoons compared to high disturbance lagoons ($p = 0.037$).

In the small deltas, pCO$_2$ was significantly higher in the very high disturbance systems ($n = 366$) compared to the high disturbance systems ($n = 353$) ($p = 0.001$), but water-air CO$_2$ flux was similar between the high and very high disturbance systems ($p = 0.101$) (Fig. 3B). No measurements were taken in low and moderate disturbance small deltas. In the tidal systems, disturbance effects on pCO$_2$ were insignificant in the low ($n = 315$) and moderate ($n = 472$) ($p = 0.682$), and low and high ($n = 117$) disturbance systems ($p = 0.118$) but significantly increased from the moderate to high disturbance systems ($p \geq 0.006$) (Fig. 3). pCO$_2$ in the very high ($n = 234$) disturbance tidal systems was significantly greater than in low disturbance systems ($p = 0.001$). Water-air CO$_2$ fluxes significantly increased with higher disturbance ($p = 0.001$) except between the low and high disturbance systems ($p = 0.094$). Water-air CO$_2$ fluxes were greatest in very high disturbance systems (Fig. 3C2 and Table 1).

Table 1 | Descriptive statistics calculated for pCO$_2$ and water-air CO$_2$ fluxes using data at per-minute resolution of each estuary type, disturbance group, and in the disturbance groups within each estuary type

Estuary type	Disturbance	pCO$_2$ (µatm) Per-minute (averaged per-estuary)						Water-air CO$_2$ flux (mmol CO$_2$-C m^{-2} d^{-1}) Per-minute (averaged per-estuary)					
		Mean	Median	SE	IQR	Min	Max	Mean	Median	SE	IQR	Min	Max
Lagoons	All	799	555	13	336	17 (334)	9478 (1906)	26.4	12.4	0.9	30.5	−64.7 (−12.6)	546.7 (85.6)
Small deltas	All	1181	1012	12	1054	344 (413)	4342 (2703)	63.9	42.9	1.1	82.8	−2.6 (2.1)	401.1 (234.1)
Tidal systems	All	1007	849	6	611	329 (585)	2906 (1611)	54.8	41.3	0.8	45.4	−3.5 (11.8)	570.8 (131.8)
All	Low	864	751	10	569	17 (457)	2162 (855)	34.1	24.2	0.8	38.0	−46.2 (0)	172.5 (48.5)
All	Moderate	869	762	9	341	116 (454)	9478 (1927)	39.7	36.4	0.6	39.9	−64.7 (−5.5)	193.8 (75.4)
All	High	977	744	11	737	233 (405)	5371 (2238)	46.6	29.8	1.1	49.9	−46 (−3)	546.7 (183.9)
All	Very high	1152	846	12	1058	199 (417)	5791 (2454)	63.8	39.1	1.2	75.9	−9.2 (2)	570.8 (187.8)
Lagoons	Low	185	163	10	285	17 (92)	436 (203)	−18.7	−18.0	0.6	5.6	−46.2 (−29)	4 (−9.5)
	Moderate	657	559	28	194	116 (378)	9478 (1980)	10.1	9.2	0.8	9.9	−64.7 (−16.9)	193.8 (48.3)
	High	859	536	22	509	233 (337)	5371 (2357)	37.7	20.7	2.0	37.8	−46 (−11.3)	546.7 (177.7)
	Very high	916	604	23	377	199 (403)	5791 (2297)	31.9	14.2	1.2	35.8	−9.2 (-0.6)	233.8 (99.7)
Small deltas	High	1063	842	16	904	350 (410)	3992 (2535)	57.2	37.1	1.6	69.9	−2.1 (0.5)	401.1 (230.9)
	Very high	1296	1245	17	1113	344 (417)	4342 (2870)	70.3	51.2	1.6	96.3	−2.6 (3.7)	374.5 (237.3)
Tidal systems	Low	956	840	9	609	577 (731)	2162 (1344)	41.3	29.1	0.7	38.2	10.9 (21.7)	172.5 (92)
	Moderate	942	822	8	411	329 (562)	2846 (1854)	49.9	43.0	0.6	30.4	−3.5 (10.6)	164.1 (113.3)
	High	981	934	17	647	406 (558)	1683 (1052)	34.6	34.2	1.0	27.4	−0.1 (7.5)	114.8 (58.2)
	Very high	1217	1067	20	1017	397 (445)	2906 (1937)	92.8	72.2	3.0	85.1	−2.4 (3.7)	570.8 (264.8)

The mean of minimum and maximum values calculated for each estuary are presented in brackets.

SE standard error, *IQR* interquartile range (3rd quartile–1st quartile).

Seasonal CO$_2$ emissions from Australian estuaries

We estimated that Australian estuaries emit a mean (±SE) of 7.62 ± 0.48 Tg CO$_2$-C yr^{-1} over the summer season, of which tidal systems contributed 93.4%, and lagoons and small deltas contributed 4.4% and 2.2%, respectively. To estimate winter water-air CO$_2$ fluxes, seasonal ratios from published summer and winter water-air CO$_2$ fluxes from 13 estuaries (Supplementary Table 1) were averaged to obtain the seasonal ratio (winter CO$_2$ flux: summer CO$_2$ flux) for each estuary type (Supplementary Table 2) which were then applied to summer water-air CO$_2$ fluxes from the current study. In these 13 estuaries, lagoons in winter had a lower mean CO$_2$ uptake, with seasonal ratios ranging from 0.58 to 0.69 (mean: 0.64; Supplementary Table 2). Small deltas and tidal systems in winter had higher mean water-air CO$_2$ flux rates than in summer, with seasonal ratios ranging from 0.33 to 4.71 in small deltas (mean: 1.49) and 0.43 to 2.17 in tidal systems (mean: 1.3) (Supplementary Table 2). Winter water-air CO$_2$ fluxes in Australian estuaries had a mean (±SE) flux rate of 49.7 ± 7.5 mmol CO$_2$-C m^{-2} d^{-1}, 25.8% higher than summer flux rates (Table 2).

Annual CO$_2$ emissions from Australian estuaries

The mean annual CO$_2$ emission from Australian estuaries was 8.67 ± 0.54 Tg CO$_2$-C yr^{-1} (Table 2), with tidal systems accounting for 94.4% of annual CO$_2$ emissions, followed by small deltas at 2.5%, and lagoons at 3.1%. These proportions compared with surface areas for tidal systems, lagoons, and small deltas, representing 89.9%, 8.6%, and 1.5% of total Australian estuary surface area, respectively (Table 3). Due to the larger surface area coverage of lagoons with increased disturbance (Table 3), CO$_2$ emissions from lagoons were dominated by the higher disturbance systems. High disturbance lagoons had the greatest CO$_2$ flux rates, but very high disturbance lagoons covered a greater proportion of lagoon surface area (62%) and therefore, as a category, emitted the most CO$_2$. In contrast, lower disturbance small deltas and tidal systems covered the largest proportion of their respective estuary-type surface area and emitted the most CO$_2$ annually (Tables 2 and 3). Low and moderately disturbed tidal systems

had the greatest total emissions, driven mainly by the large surface area coverage (33% and 48%, respectively) in remote northern Australia. Very high disturbance small deltas had the highest water-air fluxes and the largest proportion of total small delta surface area (50%) and therefore, emitted the most CO$_2$ annually. Low disturbance lagoons were the only CO$_2$ sinks of all the estuary types and disturbance groups, whereas in tidal systems the very high disturbance systems emitted the least CO$_2$ annually. The low, moderate, and high disturbance small deltas emitted similarly low levels of CO$_2$ annually (Table 2). Moderately disturbed Australian estuaries had the largest CO$_2$ emissions, followed by the high, low, and very high disturbance systems (Table 2).

Discussion

There was a strong geomorphic effect on measured pCO$_2$ and water-air CO$_2$ fluxes in Australian estuaries (Fig. 2A1 and A2), with the lagoons particularly different from the small deltas and tidal systems. Overall, lagoons had the lowest pCO$_2$ and water-air CO$_2$ fluxes of the three geomorphic types. This was likely driven by higher benthic productivity, which can result in a net autotrophic system with CO$_2$ uptake across the water-air interface[43,44] over a diurnal period[45,46]. Indeed, seagrass meadows cover an average of 18% of lagoon water areas in NSW, compared to only ~6% in small deltas and tidal systems[47]. Consistent with this, CO$_2$ undersaturation and CO$_2$ uptake have been reported in three Australian lagoons[43], as well as non-Australian marine-dominated shallow coastal systems with a large cover of benthic vegetation (e.g. refs. [44,48,49]). Freshwater input could also be a driver of pCO$_2$ and water-air CO$_2$ fluxes in estuaries; freshwater is typically supersaturated with CO$_2$ and a source of allochthonous organic matter[5,50–52] that may subsequently decompose and release CO$_2$[7,51]. However, we found poor relationships between salinity and pCO$_2$ and water-air CO$_2$ fluxes in Australian lagoons (Supplementary Fig. 2), suggesting that freshwater organic matter was not an important source of CO$_2$ in these systems. This may reflect a weak hydrological connection between lagoons and upstream rivers, which would limit
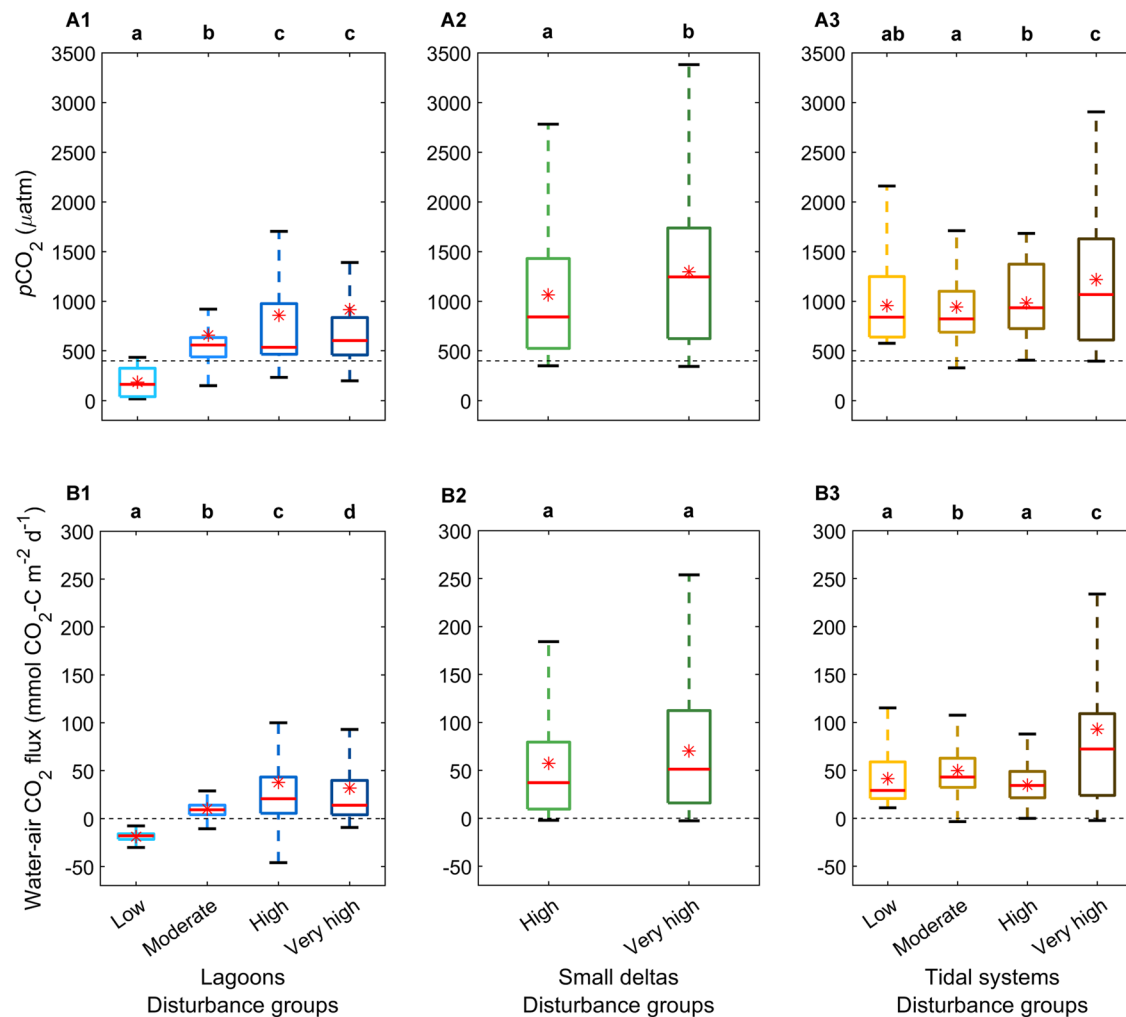
Fig. 3 | CO₂ partial pressure (pCO₂) and water-air CO₂ flux in estuary type disturbance groups. Median (red line), mean (red asterisk), 1st and 3rd inter-quartile ranges (box caps), minimum and maximum values (whiskers) of (row A) pCO_2, and (row B) water-air CO_2 flux at per-minute resolution across different disturbance groups within (column 1) lagoons (from low (light blue) to very high disturbance (dark blue), $n = 214, 815, 1312$, and 1448), (column 2) small deltas (n; high (light green)=1777, and very high (dark green)=1845), and (column 3) tidal systems (from low (light yellow) to very high disturbance (dark brown), $n = 1582$, 2374, 588, and 1176). Outliers were omitted from the figures. Dotted line along x-axis represents atmospheric pCO_2 and water-air CO_2 flux equilibrium. Letters above figures denote statistical differences among estuary types, with letters that are the same indicating no significant difference (PERMANOVA, two-tailed, and at 95% confidence interval). Source data are provided in the Source Data file.

input of riverine water. This is consistent with a previous study showing lower CO_2 emissions in estuaries with lower riverine input compared to river-dominated estuaries[53].

pCO_2 and DIC concentration were higher in small deltas and tidal systems compared to lagoons (Figure 2A1, Supplementary Fig. 4B1, Supplementary Results). The inverse relationships between salinity and pCO_2 or water-air CO_2 fluxes in small deltas and tidal systems indicate that CO_2 outgassing from the re-mineralisation of organic matter in upstream waters had a larger contribution in these systems compared to the lagoons[31], as seen in other estuaries with higher riverine input[53]. This is because increasing pCO_2 and water-air CO_2 fluxes with decreasing salinity indicate that increasing CO_2 is linked to freshwater input upstream. The tidal systems and small deltas also have a stronger connection to the river and associated input of CO_2 supersaturated water[2], which enhances CO_2 emissions in the estuary. In our study, all of the small deltas and tidal systems were tropical and sub-tropical (23.5° to 35° latitude) (Supplementary Data 1), where much of the atmospheric carbon uptake and sequestration occurs within their mangrove-lined shorelines[54,55]. Lateral export from vegetated shorelines into adjacent estuaries can be a significant pathway

for the transport of carbon in the form of DOC, POC, DIC, and CO_2-rich pore water, or as a result of the degradation of exported organic matter[56–58]. Increased tidal range resulted in an increase in pCO_2 and water-air CO_2 fluxes (Supplementary Results), suggesting increased pCO_2 and water-air CO_2 fluxes were due to lateral export in our estuaries[56–58], although we did not directly measure lateral inputs. Although estuaries in lower latitudes have higher water temperatures that could drive increased water-air CO_2 fluxes, water temperature did not correlate with pCO_2 and water-air fluxes in our estuaries (Supplementary Results). As such, higher pCO_2 and DIC concentrations in small deltas and tidal systems compared to lagoons could likely be attributed to increased lateral inorganic (and organic) carbon export from intertidal coastal wetlands due to stronger lateral exchange by tides compared to lagoons (Fig. 1E).

In contrast to the lagoons, where DIC was positively correlated with pCO_2 and water-air CO_2 fluxes, in tidal systems and small deltas pCO_2 and CO_2 fluxes were not strongly associated with DIC concentrations; only CO_2 fluxes in tidal systems showed a very weak trend with DIC concentration (Supplementary Results). Removing the effect of salinity in our analysis (as a co-variate), the differences in pCO_2 and

Table 2 | Mean, standard error (SE), and median for summer, winter, and annual water-air CO_2 flux rates and annual CO_2 emissions from Australian estuaries (Estuary (Est.) types: La: lagoons, SD: small deltas, TS: tidal systems; Disturbance (Dist.) groups: 1: low, 2: moderate, 3: high, 4: very high)

Est. type	Dist.	Summer Water-air CO_2 flux (mmol CO_2-C m^{-2} d^{-1}) Median	Mean	SE	Winter Water-air CO_2 flux (mmol CO_2-C m^{-2} d^{-1}) Median	Mean	SE	Mean (−)	Mean (+)	Annual (Summer + Winter) Water-air CO_2 flux (mmol CO_2-C m^{-2} d^{-1}) Median	Mean	SE	Mean (−)	Mean (+)	Australian CO_2 emissions (Tg CO_2-C yr^{-1}) Median	Mean	SE	Mean (−)	Mean (+)
La	1	−18.3	−18.8	0.9	−11.6	−12.0	0.6	−11.0	−13.0	−15.0	−15.4	0.8	−14.9	−15.9	−0.02	−0.02	0.00	−0.02	−0.02
	2	9.9	12.5	5.2	6.3	7.9	3.3	7.3	8.6	8.1	10.2	4.3	9.9	10.5	0.01	0.01	0.01	0.01	0.01
	3	19.5	30.4	10.8	12.4	19.3	6.9	17.7	20.9	16.0	24.8	8.8	24.0	25.6	0.05	0.08	0.03	0.07	0.08
	4	21.1	26.8	7.4	13.4	17.0	4.7	15.6	18.5	17.2	21.9	6.1	21.2	22.6	0.16	0.20	0.06	0.19	0.21
	All	12.8	16.3	5.0	8.1	10.4	3.2	9.5	11.3	10.5	13.4	4.1	12.9	13.8	0.20	0.27	0.05	0.26	0.28
SD	1[a]	–	–	–	–	–	–	–	–	–	–	–	–	–	0.03	0.03	–	0.02	0.08
	2[a]	–	–	–	–	–	–	–	–	–	–	–	–	–	0.03	0.03	–	0.02	0.07
	3	51.4	58.3	14.7	76.8	87.1	22.0	19.2	275.0	64.1	72.7	18.3	38.8	166.7	0.03	0.04	0.01	0.02	0.08
	4	61.9	70.2	10.7	92.5	104.8	15.9	23.1	330.7	77.2	87.5	13.3	46.6	200.4	0.10	0.11	0.02	0.06	0.26
	All	58.8	64.2	8.8	87.9	95.9	13.2	21.2	302.9	73.3	80.1	11.0	42.7	183.6	0.19	0.21	0.03	0.11	0.49
TS	1	44.1	46.1	12.4	57.4	60.0	16.1	19.7	100.3	50.7	53.1	14.2	32.9	73.2	2.58	2.70	0.72	1.67	3.72
	2	50.0	51.8	4.0	65.1	67.4	5.2	22.2	112.7	57.6	59.6	4.6	37.0	82.3	4.33	4.48	0.35	2.78	6.19
	3	22.2	22.2	21.8	28.9	28.9	28.4	9.5	48.3	25.6	25.6	25.1	15.9	35.3	0.63	0.63	0.62	0.39	0.87
	4	72.1	84.4	42.6	93.8	109.8	55.4	36.1	183.5	82.9	97.1	49.0	60.2	134.0	0.21	0.25	0.13	0.15	0.34
	0[b]	–	–	–	–	–	–	–	–	–	–	–	–	–	0.11	0.12	0.02	0.08	0.17
	All	49.1	52.9	10.2	63.9	68.9	13.3	22.6	115.1	56.5	60.9	11.8	37.8	84.0	7.86	8.18	0.91	5.08	11.29
All est.		36.6	39.5	5.3	35.3	49.7	7.5	16.4	116.7	31.2	44.6	6.4	27.9	78.1	8.25	8.67	0.54	5.45	12.06
All	1	23.3	18.3	14.7	30.3	29.2	16.9	6.6	51.8	26.8	23.7	15.8	12.4	35.0	1.41	1.25	0.83	0.65	1.84
All	2	29.6	28.9	6.7	18.8	32.7	9.3	13.5	52.0	24.2	30.8	7.9	21.2	40.4	1.86	2.37	0.61	1.63	3.11
All	3	36.6	42.0	9.1	44.3	52.1	14.1	17.1	142.4	40.2	47.1	11.4	29.6	92.2	1.14	1.33	0.32	0.84	2.61
All	4	51.0	55.7	10.8	65.0	70.7	16.3	22.7	176.4	54.3	63.2	13.5	39.2	116.0	0.70	0.82	0.17	0.51	1.51

Descriptive statistics for summer water-air CO_2 fluxes were calculated with per-minute resolution data measured in this study while winter water-air fluxes were calculated based on seasonal ratios. Up-adjusted means (+) (using maximum seasonal ratios) and down-adjusted means (−) (using minimum seasonal ratios) calculated from the sensitivity analysis are shown for winter and annual water-air CO_2 fluxes and annual CO_2 emissions.
[a]Mean and median low and moderate disturbance small delta annual CO_2 emissions were calculated using mean and median small delta water-air CO_2 flux rates.
[b]Mean and median annual CO_2 emissions from tidal systems with disturbance classified no assessment were calculated using mean and median tidal system water-air CO_2 flux rates.

Table 3 | Number of estuaries, estuarine surface area, and percent of total estuary surface area classified by estuary type according to Dürr et al.[2] and classified by disturbance in NLWRA[40] for sampled estuaries in this study and in all Australia

Estuary type	Disturbance	Study surface area coverage			National surface area coverage		
		Estuaries (n)	(km²)	% National representation	Estuaries (n)	(km²)	% Estuary type
Lagoons	Low	3	38	13.3	78	286	8.4
	Moderate	7	95	31.0	75	308	9.1
	High	5	226	32.1	82	704	20.8
	Very high	6	286	13.7	36	2083	61.6
	Not assessed	0	0	–	2	0	–
	Total	21	645	19.1	273	3382	8.6
Small deltas	Low	0	0	0.0	38	99	16.7
	Moderate	0	0	0.0	39	85	14.4
	High	6	18	16.3	47	112	18.9
	Very high	6	100	34.0	25	295	49.9
	Not assessed	–	–	–	0	0	–
	Total	12	119	20.1	149	591	1.5
Tidal systems	Low	4	1012	8.7	359	11598	32.7
	Moderate	5	1350	11.6	97	17152	48.4
	High	2	1553	13.4	61	5630	15.9
	Very high	3	179	1.5	27	582	1.6
	Not assessed	0	0	–	5	455	1.3
	Total	14	4094	11.6	549	35417	89.9
Total		47	4858	12.3[a]	971	39390	100
Disturbance	Estuary type	Estuaries (n)	(km²)	% National representation	Estuaries (n)	(km²)	% Disturbance group
Low	Lagoons			0.3			2.4
	Small deltas			0			0.8
	Tidal systems			8.4			96.8
	Total	7	1050	8.8	475	11983	30.4
Moderate	Lagoons			0.5			1.8
	Small deltas			0			0.5
	Tidal systems			7.7			97.8
	Total	12	1446	8.2	211	17545	44.5
High	Lagoons			3.5			10.9
	Small deltas			0.3			1.7
	Tidal systems			24.1			87.3
	Total	13	1797	27.9	190	6446	16.4
Very high	Lagoons			9.7			70.4
	Small deltas			3.4			10.0
	Tidal systems			6.0			19.7
	Total	15	565	19.1	88	2961	7.5
Not assessed	Lagoons			–			0.1
	Small deltas			–			0
	Tidal systems			0			99.9
	Total	–	–	–	7	455	1.2
Total		47	4858	12.3	971	39390	100

Two lagoons and five tidal systems were not assessed for disturbance[40].
[a]Total represented coverage of the national estuarine surface area.

water-air CO_2 flux correlations with DIC between estuary types suggests that other factors specific to small deltas and tidal systems further influence CO_2 and DIC dynamics along the estuarine gradient in those systems. For example, shorter water residence times and increased intertidal wetlands are among factors driving processes impacting CO_2 and DIC, which may include CO_2 emissions of mangrove porewater DIC and mineralisation of exported POC and DOC[55,59,60]. The positive relationship between pCO_2 and DOC (Supplementary Results and Supplementary Table 5) suggests that DOC

mineralisation may drive increased pCO_2 in small deltas. In tidal systems, stronger tidal influence compared to small deltas could further promote CO_2 emissions through the tidal resuspension of sediments, releasing DIC and organic matter for remineralisation[61–63], with excess DIC and organic matter exported to the coastal ocean[58,64].

The sensitivity analysis showed that summer:winter water-air CO_2 flux ratios ranged from 0.33 to 4.71 across the 13 estuaries (Supplementary Table 1). The largest range in summer:winter water-air flux CO_2 ratios was for small deltas, where ratios were up to 3x larger than

in lagoons and tidal systems (Supplementary Table 2). However, when estimating annual emissions, the large range in ratios in small deltas was attenuated by the large surface area of tidal systems compared to the small surface area coverage by small deltas (Table 3). Including mean winter water-air flux rates in annual Australian estuarine CO_2 emission calculations only showed 13% greater water-air flux rate and 14% greater annual emissions than from summer measurements alone. Although our study accounts for pCO_2 variations in seasonality extremes, it does not account for variations due to diurnal cycles and episodic events such as flooding. However, the diurnal effect on CO_2 emissions from estuarine surface waters is likely minimal, with differences between day and night driven more by tidal influence[65–67]. Episodic events are more significant drivers of increased CO_2 emissions in estuarine surface waters[68], but quantifying the effect of these events on CO_2 emissions in Australian estuaries was beyond the scope of this study.

The seasonal variability of water-air CO_2 fluxes in Australian estuaries is consistent with other studies globally, showing a range of change between seasons. For example, mean CO_2 water-air fluxes were highest in autumn (36.2 mmol C m^{-2} d^{-1}) (mean water temperature: 11.5 °C) followed by spring (24.1 mmol C m^{-2} d^{-1}) (7.5 °C) and summer (18.2 mmol C m^{-2} d^{-1}) (17.5 °C), and lowest in winter (7.9 mmol C m^{-2} d^{-1}) (2.9 °C) in the temperate Tay estuary (tidal system) in the United Kindom[69]. In contrast, significantly higher mean water-air CO_2 fluxes were found in winter (15.6 ± 5.2 mmol C m^{-2} d^{-1}) and summer (13.4 ± 22.2 mmol C m^{-2} d^{-1}, highest discharge rate) than in spring (−13.7 ± 16.4 mmol C m^{-2} d^{-1}) and autumn (2.7 ± 6.6 mmol C m^{-2} d^{-1}) in the Delaware Estuary, USA (tidal system) (2015 water temperature range: 0.4 °C to 28.6 °C[70], temperature data: https://waterdata.usgs.gov/monitoring-location/01463500/#parameterCode=00010&startDT=2015-01-01&endDT=2016-01-01). In the current study, there was no correlation between water-air CO_2 fluxes and temperature across all estuaries and within estuary types (studied estuary temperature range: 16 °C to 34.3 °C), except for a weak, significant correlation in tidal systems. This suggests that water-air CO_2 fluxes in our study were likely driven by factors other than temperature, for example, riverine and lateral inputs into the estuaries or residence times.

Importantly, the seasonal variability between summer and winter water-air CO_2 flux rates was small compared to the variability within individual estuaries and estuary types. Variability within the estuary types ranged from a maximum per-minute water-air CO_2 flux rate 10 times (9 times as an estuary average minimum) larger than the minimum rate in the lagoons, 156 (113) times larger in the small deltas, and 165 (13) times larger in the tidal systems (Table 1). This larger within-estuary type spatial variability in water-air CO_2 flux rates was captured in our continuous sampling along each estuary. We also accounted for the likely range of seasonal variability in water-air CO_2 flux rates (maximum in summer, minimum in winter) by applying a summer:winter ratio to our summer data. As such, we argue that our annual emissions estimates are fairly robust.

Lagoons had the strongest disturbance signal, with pCO_2 and water-air CO_2 fluxes increasing with increasing disturbance (Figure 3A1 and B1), mainly driven by changes in the extent of seagrass cover. With increasing disturbance, NSW lagoons had a general decrease in seagrass cover (low = 55%, moderate = 19%, high = 24%, and very high = 3%)[47] and mean dissolved oxygen (low = 123%$_{sat}$, moderate = 97%$_{sat}$, high = 95%$_{sat}$, and very high = 108%$_{sat}$) (Supplementary Fig. 4C2). Despite relying on data that was over 15 years old (mapped in 2007–2009)[71,72], percent seagrass cover had a strong, negative association with pCO_2 and a weaker, negative association with water-air CO_2 fluxes (Supplementary Fig. 5 and Supplementary Results). These relationships suggest that higher pCO_2 and water-air CO_2 fluxes reflect decreased CO_2 uptake by benthic vegetation (i.e. a less autotrophic system), as reported in several seagrass studies (e.g. refs. 43,44,73). High DOC concentrations in the low-disturbance
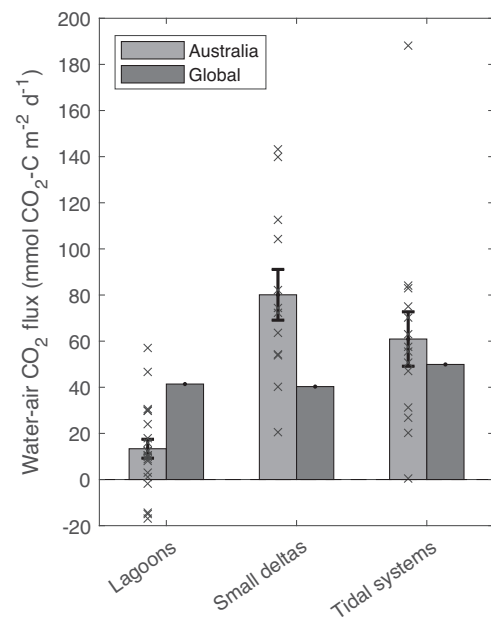
Fig. 4 | Australian and global estuarine CO_2 emissions by estuary type. Mean water-air CO_2 fluxes in Australian estuaries (n: Lagoons = 21, Small deltas = 12, and Tidal systems = 14) and in global estuaries[10] from the three estuary types defined in this study. Error bars represent standard errors. Source data are provided as a Source Data file.

lagoons were also consistent with DOC release from benthic vegetation, as observed in previous studies[48,74,75] (Supplementary Fig. 4A2, Supplementary Table 5, and Supplementary Results). High percent O_2 saturation in the very high disturbance lagoons (e.g. Curl Curl Lagoon; Supplementary Results, Supplementary Data 2, and Supplementary Table 4) was most likely due to a switch in production from benthic microalgae and macroalgae to phytoplankton[76], enabling enhanced pCO_2 drawdown and negative water-air CO_2 flux rates (Figs. 3A1, B1).

This study estimates that Australia's estuaries have a mean (±SE) annual area-weighted water-air CO_2 emissions of 44.6 ± 6.4 mmol CO_2-C m^{-2} d^{-1}, which is 25% and 110% greater, respectively, than estimates of global means of 35.6 mmol CO_2-C m^{-2} d^{-1} [10] and 21.2 mmol CO_2-C m^{-2} d^{-1} [9]. However, the role of estuary type in CO_2 flux rates had a significant impact on our estimates of Australian water-air CO_2 flux. Annual mean (±SE) area-weighted water-air CO_2 fluxes of the lagoons upscaled to all Australian lagoons (13.4 ± 4.1 mmol CO_2-C m^{-2} d^{-1}) was 68% lower than from global lagoon estimates (41.4 mmol CO_2-C m^{-2} d^{-1})[10]. In contrast, annual mean water-air CO_2 fluxes (Table 2 and Fig. 4) scaled to all Australian small deltas (80.1 ± 11 mmol CO_2-C m^{-2} d^{-1}) and tidal systems (60.9 ± 11.8 mmol CO_2-C m^{-2} d^{-1}) were 99% and 22% higher, respectively, than from global small deltas (40.3 mmol CO_2-C m^{-2} d^{-1}) and tidal systems (49.9 mmol CO_2-C m^{-2} d^{-1})[10]. In addition to the higher water-air CO_2 fluxes in Australian small deltas and tidal systems, the lower global mean water-air CO_2 flux for all estuaries combined compared to Australia likely also reflects the contribution of fjords and fjards to global estimates[9,10]. Globally, fjords and fjards have been shown to take up CO_2 from the atmosphere (median 66 Tg CO_2 yr^{-1})[11], but are absent in Australia.

Lower mean CO_2 emissions in Australian lagoons compared to lagoons globally are likely due to overall lower disturbance in Australia. In addition, it may also reflect the greater abundance of ICOLLs in Australia (21% of global occurrence[41,77,78]). Isolation from marine waters, low riverine flow, and long residence times in ICOLLs may enhance autotrophic drawdown of CO_2 by abundant seagrasses,

resulting in smaller water-air CO_2 fluxes (Table 2) than observed in non-Australian lagoons[43,79,80]. The weak hydrological connection between ICOLLs and rivers would also limit the input of CO_2 supersaturated river water.

Higher mean water-air CO_2 fluxes in Australian subtropical and tropical small deltas and tidal systems, compared to small deltas and tidal systems globally was an unexpected finding. Subtropical and tropical estuaries have previously been estimated to have lower water-air CO_2 fluxes than systems at temperate latitudes[9]. We were unable to explicitly test for climate as we do not have sufficient estuaries of each geomorphic type and disturbance in each climate zone. However, macrotidal northern Australian small deltas and tidal systems are different from the small deltas and tidal systems in previous studies[81] (Fig. 6 in Matthews and Matthews[82]) as North Australian tidal systems are dominated by extensive mangrove cover and have significantly greater tidal ranges (>4 m). Larger tidal ranges would lead to greater lateral inorganic and organic carbon export from mangroves to the tidal systems[56,58,83]. Higher mean water-air CO_2 fluxes may also reflect the longer residence times resulting from characteristically low Australian freshwater inflows[84,85]. Long residence times would allow more time for CO_2 produced from lateral inputs of DIC, DOC, and POC, and DIC from increased DOC and POC decomposition to be emitted across the water-air interface rather than flushed to the ocean.

Collectively, estuary geomorphic type is more important than disturbance in Australia, resulting in higher mean CO_2 emissions from Australian estuaries despite their lower overall disturbance compared to global estuaries. The climate zone also has an important control on estuarine geomorphic type (e.g. tropical and subtropical mangrove-dominated macrotidal estuaries). This study suggests that relative to their surface area, Australian estuaries contribute a disproportionately large amount of CO_2 emissions annually to global estuarine emissions. Using surface area estimates for Australian (62,100 km^2; calculated from Table 3 in Chen et al.[9]) and global estuaries (1,012,440 km^2) and global estuarine CO_2 emission estimates by Laruelle et al.[10] and Chen et al.[9], Australian estuaries emit a mean (±SE) of 12.1 ± 1.7 Tg CO_2-C annually. These emissions account for 12% or 8% of the estimated mean global estuarine CO_2 emissions of 0.1 Pg CO_2-C yr^{-19} or 0.15 Pg CO_2-C yr^{-110}, despite Australian estuaries accounting for only 6.1% of their calculated global estuarine surface area. This estimate includes the surface area coverage of the estuary types and disturbance groups and is dependent on the accuracy of surface areas for Australian and global estuaries. For instance, total estuarine water area of 39,390 km^2 has been reported for Australia (Table 3)[40], which is 57% greater than estimated by Dürr et al.[2] (25,056 km^2) and 37% smaller than estimated by Laruelle et al.[10] (62,100 km^2). Applying the estuarine surface areas of Australia's National Land and Water Resources Audit (NLWRA)[40] to data collected in the current study, Australian estuaries are estimated to emit (mean ± SE) 8.67 ± 0.54 Tg CO_2-C annually (Table 2).

Australian tidal systems contributed the majority of the mean (±SE) annual CO_2 emissions (8.18 ± 0.91 Tg CO_2-C yr^{-1}, 94.4%), with far smaller contributions from lagoons and small deltas (Table 2). Although lagoons in Australia (8.6% of total area) cover six times the estuarine surface area of small deltas (1.5% of total area;), CO_2 emissions from lagoons were disproportionately low (0.27 ± 0.05 Tg CO_2-C yr^{-1}, 3.1% of Australian estuarine emissions) compared to small deltas (0.21 ± 0.03 Tg CO_2-C yr^{-1}, 2.5%) reflecting smaller water-air fluxes in lagoons (Table 2). The proportions of CO_2 emitted by the different geomorphic types of estuaries in Australia were different from the proportions reported globally. For example, lagoons globally account for a larger proportion of CO_2 emissions (31%; 0.046 Pg CO_2-C yr^{-1}) than small deltas (13%; 0.019 Pg CO_2-C yr^{-1}), and tidal systems only contribute 41% of global emissions (0.063 Pg CO_2-C yr^{-1})[10]. The remaining proportion is made up of limited or non-filtering estuary types such as large rivers, karst-dominated coasts, and arheic coasts[2]. Furthermore, global CO_2 emission estimates incorporate the

contribution of fjords and fjards, which have the lowest water-air CO_2 flux or show CO_2 uptake but account for close to half of the global estuarine surface area[10,11]. Therefore, differences in Australian and global estuarine CO_2 emissions are driven mostly by the geomorphic type (related to the climate zone of the estuary). This highlights the need to include geomorphic types in global CO_2 emission assessments.

Geomorphology and disturbance influence water-air CO_2 fluxes in Australian estuaries as a result of decreased hydrological connectivity in lagoons, and increased upstream riverine lateral inputs and tidal influence in small deltas and tidal systems. Water-air CO_2 flux rates increase with higher disturbance, but geomorphology and disturbance interact, with the strongest disturbance signal in the lagoons, and a weak disturbance signal in the small deltas and tidal systems. Seasonal variations in CO_2 emissions were a less important control on water-air CO_2 fluxes in Australian estuaries. Previous global estuarine CO_2 emission estimates have included geomorphology[9–11], but not disturbance or the two factors together. CO_2 emissions for global lagoons could therefore be over-estimated due to the bias towards more disturbed systems in the northern hemisphere. In contrast, CO_2 emissions for global small deltas and tidal systems could be under-estimated due to the bias towards temperate systems in the northern hemisphere. As such, upscaling of global estuarine CO_2 emissions should be based on geomorphic estuary-types but also consider land-use disturbance and climate and ideally, their interaction with geomorphic type.

Methods
In 36 estuaries around Australia, pCO_2, DIC, DOC, physicochemistry, and physical parameters (wind speed, depth, current velocity, and barometric pressure) were measured along the salinity gradient from the marine to freshwater endmember (where possible). Data were combined with published CO_2 fluxes and water quality data for 11 other Australian estuaries[12,30], giving a total of 47 Australian estuaries. The same survey methods were used in all 47 estuaries. pCO_2 and water-air CO_2 fluxes were classified according to estuary type (lagoons, small deltas, and tidal systems) and disturbance group (low, moderate, high, and very high) and analysed for significant differences. Finally, the classified water-air CO_2 fluxes were upscaled to all of Australia and mean estimates were compared to previous global mean estimates of estuary CO_2 emissions. While we provide a full set of statistics in this study, we use the mean (±SE) for global comparison because our high-resolution water-air CO_2 fluxes over a range of disturbance classes and geomorphic estuary types was better represented by the means than medians.

Estuary classification schemes
Estuaries were selected to cover a large range of disturbance and geomorphic types according to the classifications of NLWRA[40] and Dürr et al.[2]. NLWRA[40] assessed 971 Australian estuaries and described four disturbance classes (low (near-pristine), moderate (relatively unmodified), high (modified), and very high (extensively modified)). These disturbance groups were qualitatively classified based on changes in catchment land-use, estuary use, and ecology (Supplementary Table 6) and provided an assessment that was more relevant than adopting a single set of indicators. This is because the Australian continent covers a large surface area, encompassing over 1000 estuaries and climatic variations, making a single set of disturbance indicators likely misleading[86,87]. The global estuarine typology of Dürr et al.[2] details three geomorphic types found in Australia: (1) lagoons (including Intermittently Closed or Open Lakes and Lagoons (ICOLLs) and estuaries with a central basin morphology), (2) small deltas, and (3) tidal systems (including drowned river valleys and tidal embayments), based around morphological and sedimentation characteristics driven by tidal influence (classification criteria in Supplementary Table 7). However, the existing classification of Australian estuaries[2] did not match our observations of satellite imagery, because it was developed
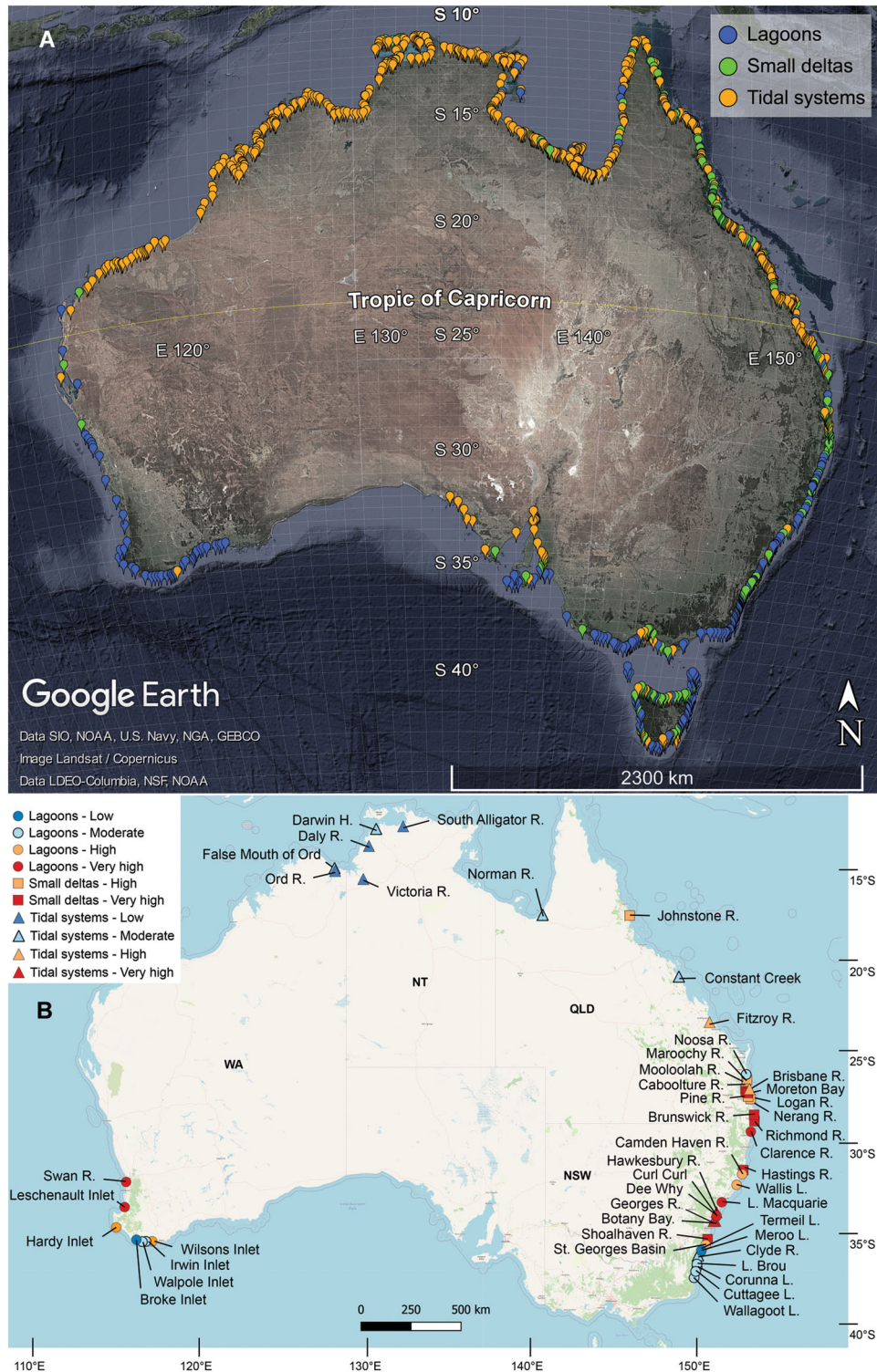
Fig. 5 | Distribution of estuary types and study locations in Australia.
A Estuaries in Australia[40] classified into three estuary types based on conceptual definitions (Supplementary Table 7) by Dürr et al.[2] (©Google Earth) and the (**B**) location of study estuaries in Australia according to estuary type (shapes) and disturbance class (colours) (©OpenStreetMap, https://www.openstreetmap.org/copyright). H.: Harbour, R.: River, and L.: Lake.

with a low spatial resolution (0.5°, or 50 km). Therefore, all 971 Australian estuaries were re-classified into the three estuary types by distinguishing physical characteristics based on the criteria of Dürr et al.[2] (Supplementary Table 7) using satellite imagery (Google Earth) (Supplementary Data 3). Water surface area for 108 estuaries with missing surface area measurements were also calculated using satellite

imagery (Google Earth). The re-classified estuary database was then combined with the estuarine disturbance database in NLWRA[40] (dataset URL: https://data.gov.au/dataset/ds-aodn-8fec03d6-48e3-4352-9ddb-085e42e55637/details?q=, Supplementary Data 3).

The spatial distribution of estuary types in Australia corresponds to the tidal ranges of their respective coastlines (Fig. 5A). Tidal systems

dominate the macro-tidal regions of northern Australia, whereas lagoons are found mostly in the micro-tidal regions of southern Australia. All three estuary types with all four disturbance groups, except for low and moderate disturbance in small deltas, were included in our estuary selection (Table 3). The surface area of estuaries sampled and included in this study represents 12.3% of the total Australian estuarine surface area, consisting of 19.1% of lagoons, 20.1% of small deltas, and 11.6% of tidal systems in Australia (Table 3).

Study sites

Measurements from the 36 estuary surveys and from the 11 published estuary surveys were taken over the austral spring-summer season (Fig. 5B and Supplementary Data 1). The estuaries included in this study were comprised of 21 estuaries in New South Wales (Nov to Dec 2017), one in southeast Queensland (Moreton Bay, Oct 2018), seven along the north Australian coastline (from Karumba, Queensland to Wyndham, Western Australia, Oct to Dec 2018), seven along the southwest coastline of Western Australia (from Albany to Perth, Feb to Mar 2019), three in north-east Queensland[30] (late spring Sept to Oct 2014) and eight in southeast Queensland[12] (late spring Oct 2016) (Fig. 5B and Supplementary Data 1). Percent seagrass coverage for the New South Wales estuaries was obtained from Roper et al.[47]. Termeil Lake and Lake Brou were excluded from seagrass coverage analysis because although zero coverage was recorded by Roper et al.[47], extensive seagrass cover was observed during our surveys.

Underway data measurements

Using a 6 m research vessel, physicochemical parameters and pCO_2 were measured along a transect encompassing the length of each of the 36 estuaries, starting at the river mouth just after high-tide and ending in freshwater (salinity ~2). Although we aimed to finish the surveys at salinity ~2, this was not always possible because of shallow water and/or natural and artificial obstacles. As such, estuary data in this study reflect the spatial variations along the estuarine gradient (marine to upstream-riverine). A cruising ground speed of ~8 km h^{-1} was maintained where possible to ensure spatial and temporal consistency. The surveys were carried out during daylight hours, typically lasting over the course of a day. Surveys in large estuaries often required 2 to 3 days but never exceeded five days (Supplementary Data 1). pCO_2 was recorded at one-minute intervals using an integrated water-gas loop setup (Supplementary Fig. 6).

Water was continuously pumped from beneath the hull (0.5 m to 1 m water depth) at ~1800 l^{-1} h^{-1} using a 12 V pump with backflow prevention (800GPH, Rule) to a high-flow filter basket (Ozito) before entering a two-way split. One path led to a flow-through chamber with a multi-parameter sonde (HL4, Hydrolab) measuring salinity (±0.5%), temperature (±0.1 °C), pH$_{NBS}$ (±0.2), and dissolved oxygen (DO$_{\%sat}$; ±2%). The second path entered a loop consisting of a pair of interconnected showerhead exchangers (RAD Aqua, Durridge) equilibrating dissolved gases in the water with the headspace. The dried gas stream was then measured for CO_2 concentration, using a LiCOR 840 A CO_2 gas analyser (accuracy <1%) and a Picarro G-2508 Cavity Ring-Down Spectrometer (CRDS, ±0.05%)[87]. In the ICOLL lagoons (indicated in Supplementary Data 1) where a smaller boat was used, CO_2 measurements were only taken with the LiCOR 840 A CO_2 gas analyser. Measured CO_2 was humidity-corrected and in-situ pCO_2 was calculated using methods in Pierrot et al.[88]. The LiCOR 840 A was calibrated using a two-step process with low (250 ppm) and high (8000 ppm) pCO_2 gas standards. The CRDS was serviced and calibrated by the manufacturer (Picarro, USA) before each field trip.

Discrete water samples, morphological, and meteorological data

Water samples were collected for DIC and DOC concentrations, along with estuarine (depth and water current velocity) and meteorological

measurements at the start and end of survey transects and at salinity intervals of ~5. In cases where salinity did not change much (<5) along the survey, samples were collected every hour instead (i.e. every 8 km of estuary travelled). In the ICOLL lagoons (as indicated in Supplementary Data 1) where no significant salinity gradient was present, discrete water samples were collected from at least 3 points across the estuary. For DOC, 30 ml water samples were filtered through a pre-combusted (500 °C, ~5 h) 0.7 μm GF/F filter (Whatman, Merck) into an acid-washed glass vial containing 100 μl of 85% phosphoric acid (H$_3$PO$_4$). 50 ml water samples for DIC analysis were syringe-filtered (0.45 μm SFCA Minisart, Sartorius) into a crimp-top glass bottle without any headspace and preserved with 30 μl mercuric chloride (HgCl$_2$). DOC concentrations were determined using a total organic carbon analyser (±3%; 1030 W, Aurora)[89]. DIC concentrations were analysed with a Marianda AIRICA coupled to a CO_2/H$_2$O analyser (LI7000, LiCOR), calibrated for accuracy with certified reference material[90] at a typical precision of better than 2 μmol kg^{-1} [91]. All samples were processed immediately, stored on ice while the survey was underway, and frozen (−20 °C) as soon as possible (typically within five hours of collection) except for DIC, which was stored at room temperature. On the main research vessel and the smaller boat, water current velocity was measured using a differential GPS-assisted Lagrangian method with a neutrally-buoyant drifter (adapted from Wetzel and Likens[92]). Current velocity measurements likely indicated flow rates of the ebbing tide, as the surveys were carried out after the turn of the high tide. Water depth on the main research boat was measured using a hull-mounted acoustic transducer (Airmar), while water depth was measured using a lead and line on the smaller boat or taken from Roper et al.[47]. Barometric pressure (±0.5hPa @20 °C), air temperature (±1.1 °C @20 °C), and true wind speed (±5% @10 m s^{-1}) were measured 3 m above the water surface using a vessel-mounted weather station (200WX, Airmar). In the ICOLL lagoons, daily averaged meteorological data were obtained from the closest Bureau of Meteorology (BOM) weather station (Climate Data Online[93]).

Water-air CO$_2$ flux calculations

Water-air CO_2 flux (FCO_2; mmol CO_2-C m^{-2} d^{-1}) was calculated at 1-minute intervals using Eq. (1):

$$F = k_{600}K_0(C_{water} - C_{air}) \qquad (1)$$

where k_{600} is the gas transfer velocity (m d^{-1}), K_0 is the solubility coefficient of CO_2 (mol l^{-1} atm^{-1}), and C_{water} and C_{air} are the partial pressure of CO_2 (μatm) in water and air, respectively[94]. The formula from Weiss[95] was used to obtain CO_2 solubility coefficients based on salinity and temperature Eq. (2):

$$ln K_0 = A_1 + A_2\left(\frac{100}{T}\right) + A_3 ln\left(\frac{T}{100}\right) + S\left[B_1 + B_2\left(\frac{T}{100}\right) + B_3\left(\frac{T}{100}\right)^2\right] \qquad (2)$$

where K_0 is expressed in moles L^{-1} atm^{-1}, A_1 (-58.0931), A_2 (90.5069), A_3 (22.2940), B_1 (0.027766), B_2 (-0.025888), and B_3 (0.0050578) are constants, T is absolute temperature, and $S‰$ is the salinity. CO_2 atmospheric concentration was assumed to be 407 μatm[96], which was the mean concentration in 2018. Although k_{600} is a significant variable required for calculating water-air fluxes, measuring k_{600} in-situ was not feasible due to the large spatial coverage of this study. As such, five empirical k_{600}-models for a range of coastal-marine ecosystems were used from the literature to estimate mean k_{600} (equations (6) to (10) listed in Table 4), i.e., mangrove-dominated[28,97] and tidal[27] (using wind speed, water depth, and current velocity), lagoonal[53] (using wind speed and water depth), and marine-dominated[94] (using wind speed only) coastal ecosystems. Windspeed is corrected for a height of 10 m (U_{10}) by rearranging the formula

Table 4 | Gas transfer velocity normalised to Schmidt number of 600 (k_{600}) parameterisations using various methods in published literature

Literature	k_{600} parameterisations	Method	Study area	Eqn.
Rosentreter et al.[97]	$k_{600} = -0.08 + 0.26\,v + 0.83U_{10} + 0.59\,h$	Flux chamber	Three mangrove estuaries	6
Borges et al.[27]	$k_{600} = 1 + 1.719v^{0.5}\,h^{-0.5} + 2.58U_{10}$	Flux chamber	Macrotidal estuary (Scheldt)	7
Jiang et al.[53]	$k_{600} = 0.314\,U_{10}^2 - 0.436U_{10} + 3.99$	Predictive modelling	Global	8
Ho et al.[28].	$k_{600} = 0.77\,v^{0.5}\,h^{-0.5} + 0.266U_{10}$	$^3He/SF_6$	Mangrove estuaries	9
Wanninkhof[94]	$k = 0.251U_{10}^2\,(Sc/660)^{-0.5}$	Global ocean inverse model	Global	10

v is the current velocity in cm s^{-1}, h is the water depth (m), and U_{10} is the wind speed (m s^{-1}) at 10 m height calculated according to Amorocho and DeVries[98].

from Amorocho and DeVries[98]:

$$U_z = U_{10}\left[1 - \frac{(C_{10})^{\frac{1}{2}}}{k}\ln\left(\frac{10}{z}\right)\right] \tag{3}$$

where U_z is the measured windspeed at z height (3 m) in m s^{-1}, C_{10} is the surface drag coefficient for wind at 10 m (1.3×10^{-3}[97]), and κ is the Von Karman constant (0.41). In the first four parameterisations (Eqs. (6) to (9) in Table 4), k_{600} is the gas transfer velocity (cm h^{-1}) normalised to a Schmidt number of 600. The parameterisation in equation 10 (Table 4) by Wanninkhof[94] calculated k at the Schmidt number (Sc) of the measured temperature and salinity, converted to k_{600} using Eq. (4):

$$k_{600} = k\left(\frac{600}{Sc}\right)^{-0.5} \tag{4}$$

A Schmidt exponent of -0.5 was used to account for higher water turbulences associated with tidal currents in estuaries[99]. To calculate water-air CO_2 fluxes, k was derived from k_{600}, which was calculated using the other four parameterisations (Eqs. (6) to (9) in Table 4) by rearranging Eq. (4). Sc at the measured temperature and salinity was calculated using the formula in Wanninkhof[94] (Eq. (5)):

$$Sc = A + Bt + Ct^2 + dt^3 + Et^4 \tag{5}$$

where A, B, C, D, and E are constants for CO_2 in fresh water (1923.6, −125.06, 4.3773, −0.085681, and 0.00070284, respectively) and seawater (2116.8, −136.25, 4.7353, −0.092307, 0.0007555, respectively), and t is temperature in °C. A salinity factor was calculated from the difference between freshwater and sea water Sc and applied to calculate Sc at the measured salinity.

To ensure consistency between water-air CO_2 fluxes measured for estuaries in this study and those previously reported for eight southeast Queensland estuaries[12], water-air CO_2 fluxes were recalculated using the five parameterisations. Water-air CO_2 fluxes from the previously reported three north Queensland estuaries[30] were not recalculated because water depth and current velocity data were unavailable. However, given that these three estuaries were each categorised in a different disturbance group and/or estuary type (moderate and high disturbance tidal system, and a high disturbance small delta, Table 3), this should not introduce any systematic bias.

Data processing and statistical analysis
Per-minute pCO_2 and water-air CO_2 flux were averaged to 5-minute datapoints to reduce the number of data points whilst maintaining the high resolution and main features of the dataset. Kolmogorov-Smirnov and Levene's tests for normality and homoscedasticity, respectively, returned significant results ($p < 0.05$), ruling out parametric methods for statistical analysis. Consequently, significant differences ($\alpha = 0.05$) between and within estuary types (3 factors) and disturbance groups

(4 factors) were tested using the Permutational Multivariate Analysis of Variance (PERMANOVA) procedure with Euclidean distance as the dissimilarly matrix in Primer v7 and PERMANOVA+ add-on (PRIMER-e). The dataset for PERMANOVA analysis was normalised (z-score) but not power-transformed to retain the heterogeneity between the mean and variances, retaining the spatial scale along the estuarine transect. Not power-transforming the data reduces the possibility of an inflated type I error[100]. Salinity was included as a covariate in the pCO_2, water-air CO_2 flux, DOC and DIC analyses to remove differences influenced by salinity. The focus of PERMANOVA is on the differences between the data points rather than descriptive statistics (mean, median, etc.). PERMANOVA can therefore, identify significant differences in datasets even where there are similarities in the descriptive statistics. 9999 permutations were performed using residuals under a reduced model using type I sum of squares. Significant results were further analysed with pairwise PERMANOVA. pCO_2 and water-air CO_2 fluxes were analysed for correlations with salinity using Pearson's correlation and combined with physicochemical data, DOC, DIC, and percent seagrass cover to analyse for partial correlations while controlling for the effect of salinity ($\alpha = 0.05$) in SPSS v25 (IBM). Data used for correlation analysis were power-transformed where necessary and normalised (z-score). Partial correlation analysis was chosen over multivariate methods such as Principal Component Analysis (PCA) because targeted testing for correlations between variables and CO_2 was more useful than an exploratory approach.

CO_2 emission upscaling to the Australian continent
Published summer and winter water-air CO_2 flux rates were available for 13 Australian estuaries, including each of the three geomorphic estuary types (Supplementary Table 1). Of these, 10 of the estuaries were included in this study[12,30], along with an additional three from a published study[43]. The summer and winter water-air CO_2 fluxes were used to calculate a summer:winter water-air CO_2 flux ratio (mean and range) for each of the three estuary types (Supplementary Table 2). Ratios for each estuary type were then applied to the measured summer water-air CO_2 fluxes for the 47 estuaries to estimate the mean and range of winter water-air CO_2 fluxes (Table 2). The summer and winter mean water-air CO_2 flux rates from each estuary were averaged together to derive the annual water-air CO_2 flux rates and emissions for the 47 estuaries. To gauge the sensitivity of annual Australian emissions to winter flux rates, the summer mean flux rates were also adjusted up and down by the minimum and maximum of winter:summer ratios (Supplementary Table 2). Upscaled fluxes determined based on these minimum and maximum ratios allow an upper and lower limit to be placed on these estimates.

Annual CO_2 emissions from the 47 estuaries were upscaled to all Australian estuaries ($n = 971$) by multiplying the estuary type-specific and disturbance-specific water-air CO_2 fluxes (mmol CO_2-C m^{-2} d^{-1}) by the total estuarine surface area of the relevant systems[40] (Table 3). Small deltas with low to moderate disturbance were not available for this study. However, even though measured low and moderately disturbed small delta water-air CO_2 fluxes were likely different from the

mean high and very high disturbed small delta water-air CO_2 flux, their impact on total Australian estuary emissions is low. This is because small deltas only make up 1.5% of Australia's estuarine surface area (Table 3).

Reporting summary

Further information on research design is available in the Nature Portfolio Reporting Summary linked to this article.

Data availability

The environmental survey data generated/used in this study is freely available and has been deposited in the FigShare database under accession code https://doi.org/10.6084/m9.figshare.25242676. Figure source data are provided with this paper as part of the Supplementary Information. Source data are provided with this paper.

References

1. Regnier, P., Resplandy, L., Najjar, R. G. & Ciais, P. The land-to-ocean loops of the global carbon cycle. *Nature* **603**, 401–410 (2022).
2. Dürr, H. H. et al. Worldwide typology of nearshore coastal systems: defining the estuarine filter of river inputs to the oceans. *Estuaries and Coasts* **34**, 441–458 (2011).
3. Rosentreter, J. A. et al. Half of global methane emissions come from highly variable aquatic ecosystem sources. *Nat. Geosci.* **14**, 225–230 (2021).
4. Takahashi, T. et al. Climatological mean and decadal change in surface ocean pCO2, and net sea-air CO2 flux over the global oceans. *Deep. Res. Part II Top. Stud. Oceanogr.* **56**, 554–577 (2009).
5. Regnier, P. et al. Anthropogenic perturbation of the carbon fluxes from land to ocean. *Nat. Geosci.* **6**, 597–607 (2013).
6. Cai, W. J. Estuarine and coastal ocean carbon paradox: CO2 sinks or sites of terrestrial carbon incineration? *Ann. Rev. Mar. Sci.* **3**, 123–145 (2011).
7. Borges, A. V. & Abril, G. in *Treatise on Estuarine and Coastal Science* (eds. Wolanski, E. & McLusky, D.) Vol. 5, 119–161 (Academic Press, 2011).
8. Bauer, J. E. et al. The changing carbon cycle of the coastal ocean. *Nature* **504**, 61–70 (2013).
9. Chen, C. T. A. et al. Air-sea exchanges of CO2 the world's coastal seas. *Biogeosciences* **10**, 6509–6544 (2013).
10. Laruelle, G. G. et al. Global multi-scale segmentation of continental and coastal waters from the watersheds to the continental margins. *Hydrol. Earth Syst. Sci.* **17**, 2029–2051 (2013).
11. Rosentreter, J. A. et al. Coastal vegetation and estuaries collectively are a greenhouse gas sink. *Nat. Clim. Chang.* **13**, 579–587 (2023).
12. Wells, N. S. et al. Land-use intensity alters both the source and fate of CO_2 within eight sub-tropical estuaries. *Geochim. Cosmochim. Acta* **268**, 107–122 (2020).
13. Nguyen, A. T. et al. Does eutrophication enhance greenhouse gas emissions in urbanized tropical estuaries? *Environ. Pollut.* **303**, 119105 (2022).
14. David, F. et al. Carbon biogeochemistry and CO2 emissions in a human impacted and mangrove dominated tropical estuary (Can Gio, Vietnam). *Biogeochemistry* **138**, 261–275 (2018).
15. Looman, A. et al. Dissolved carbon, greenhouse gases, and δ 13 C dynamics in four estuaries across a land use gradient. *Aquat. Sci.* **81**, 1–15 (2019).
16. Frankignoulle, M., Abril, G., Borges, A., Bourge, I., Canon, C., Delille, B., Libert, E. & Théate, J.-M. Carbon dioxide emission from european estuaries. *Science* **282**, 434–436 (1998).
17. Raymond, P. A., Saiers, J. E. & Sobczak, W. V. Hydrological and biogeochemical controls on watershed dissolved organic matter transport: Pulse- shunt concept. *Ecology* **97**, 5–16 (2016).
18. Poff, N. L. R., Olden, J. D., Merritt, D. M. & Pepin, D. M. Homogenization of regional river dynamics by dams and global biodiversity implications. *Proc. Natl Acad. Sci. USA.* **104**, 5732–5737 (2007).
19. Borges, A. V. et al. Effects of agricultural land use on fluvial carbon dioxide, methane and nitrous oxide concentrations in a large European river, the Meuse (Belgium). *Sci. Total Environ.* **610–611**, 342–355 (2018).
20. Asmala, E. et al. Bioavailability of riverine dissolved organic matter in three Baltic Sea estuaries and the effect of catchment land use. *Biogeosciences* **10**, 6969–6986 (2013).
21. Asmala, E., Kaartokallio, H., Carstensen, J. & Thomas, D. N. Variation in riverine inputs affect dissolved organic matter characteristics throughout the estuarine gradient. *Front. Mar. Sci.* **2**, 1–15 (2016).
22. Jennerjahn, T. C. et al. Effect of land use on the biogeochemistry of dissolved nutrients and suspended and sedimentary organic matter in the tropical Kallada River and Ashtamudi estuary, Kerala, India. *Biogeochemistry* **90**, 29–47 (2008).
23. Tanner, E. L., Mulhearn, P. J. & Eyre, B. D. CO_2 emissions from a temperate drowned river valley estuary adjacent to an emerging megacity (Sydney Harbour). *Estuar. Coast. Shelf Sci.* **192**, 42–56 (2017).
24. Dinauer, A. & Mucci, A. Spatial variability in surface-water pCO2 and gas exchange in the world's largest semi-enclosed estuarine system: St. Lawrence Estuary (Canada). *Biogeosciences* **14**, 3221–3237 (2017).
25. Dalrymple, R. W., Zaitlin, B. A. & Boyd, R. Estuarine facies models: conceptual basis and stratigraphic implications. *J. Sediment. Petrol* **62**, 1130–1146 (1992).
26. Boyd, R., Dalrymple, R. & Zaitlin, B. A. Classification of clastic coastal depositional environments. *Sediment. Geol.* **80**, 139–150 (1992).
27. Borges, A. V. et al. Variability of the gas transfer velocity of CO_2 in a Macrotidal Estuary (the Scheldt). *Estuaries* **27**, 593–603 (2004).
28. Ho, D. T. et al. Influence of current velocity and wind speed on air-water gas exchange in a mangrove estuary. *Geophys. Res. Lett.* **43**, 3813–3821 (2016).
29. Zappa, C. J. et al. Environmental turbulent mixing controls on air-water gas exchange in marine and aquatic systems. *Geophys. Res. Lett.* **34**, 1–6 (2007).
30. Rosentreter, J. A., Maher, D. T., Erler, D. V., Murray, R. H. & Eyre, B. D. Factors controlling seasonal CO_2 and CH_4 emissions in three tropical mangrove-dominated estuaries in Australia. *Estuar. Coast. Shelf Sci.* **215**, 69–82 (2018).
31. Borges, A. V. Do we have enough pieces of the jigsaw to integrate CO_2 fluxes in the Coastal Ocean? *Estuaries* **28**, 3–27 (2005).
32. Koné, Y. J. M., Abril, G., Kouadio, K. N., Delille, B. & Borges, A. V. Seasonal variability of carbon dioxide in the rivers and lagoons of ivory coast (West Africa). *Estuaries and Coasts* **32**, 246–260 (2009).
33. Erbas, T., Marques, A. & Abril, G. A CO_2 sink in a tropical coastal lagoon impacted by cultural eutrophication and upwelling. *Estuar. Coast. Shelf Sci.* **263** (2021).
34. Cotovicz, L. C., Knoppers, B. A., Brandini, N., Costa Santos, S. J. & Abril, G. A strong CO_2 sink enhanced by eutrophication in a tropical coastal embayment (Guanabara Bay, Rio de Janeiro, Brazil). *Biogeosciences* **12**, 6125–6146 (2015).
35. Bianchi, T. S. *Biogeochemistry of Estuaries. Biogeochemistry of Estuaries* (Oxford University Press, 2007).
36. Maher, D. T., Santos, I. R., Golsby-Smith, L., Gleeson, J. & Eyre, B. D. Groundwater-derived dissolved inorganic and organic carbon exports from a mangrove tidal creek: the missing mangrove carbon sink? *Limnol. Oceanogr.* **58**, 475–488 (2013).

37. Luijendijk, E., Gleeson, T. & Moosdorf, N. Fresh groundwater discharge insignificant for the world's oceans but important for coastal ecosystems. *Nat. Commun.* **11**, 1–12 (2020).

38. Valerio, A. M. et al. CO_2 partial pressure and fluxes in the Amazon River Plume using in situ and remote sensing data. *Cont. Shelf Res.* **215** (2021).

39. Chen, C. T. A., Huang, T. H., Fu, Y. H., Bai, Y. & He, X. Strong sources of CO_2 in upper estuaries become sinks of CO_2 in large river plumes. *Curr. Opin. Environ. Sustain* **4**, 179–185 (2012).

40. NLWRA. *Australian Catchment, River and Estuary Assessment 2002* Vol. 1 (National Land and Water Resources Audit, Commonwealth Government, 2002).

41. McSweeney, S. L., Kennedy, D. M., Rutherfurd, I. D. & Stout, J. C. Intermittently Closed/Open Lakes and Lagoons: Their global distribution and boundary conditions. *Geomorphology* **292**, 142–152 (2017).

42. Regional population, Australia, 2020-2021. *Australian Bureau of Statistics* https://www.abs.gov.au/statistics/people/population/regional-population/2020-21 (2022).

43. Maher, D. T. & Eyre, B. D. Carbon budgets for three autotrophic Australian estuaries: Implications for global estimates of the coastal air-water CO 2 flux. *Global Biogeochem. Cycles* **26** (2012).

44. Chen, J. J., Wells, N. S., Erler, D. V. & Eyre, B. D. Importance of habitat diversity to changes in benthic metabolism over land-use gradients: evidence from three subtropical estuaries. *Mar. Ecol. Prog. Ser.* **631**, 31–47 (2019).

45. Ollivier, Q. R., Maher, D. T., Pitfield, C. & Macreadie, P.I. Net drawdown of greenhouse gases (CO_2, CH_4 and N_2O) by a temperate Australian seagrass meadow. *Estuaries Coasts* **45**, 2026–2039 (2022).

46. Ganguly, D. et al. Seagrass metabolism and carbon dynamics in a tropical coastal embayment. *Ambio* **46**, 667–679 (2017).

47. Roper, T. et al. *Assessing the Condition of Estuaries and Coastal Lake Ecosystems in NSW, Evaluation and Reporting Program, Technical Report Series Estuaries and Coastal Lakes* (2011).

48. Banerjee, K. et al. Seagrass and macrophyte mediated CO_2 and CH_4 dynamics in shallow coastal waters. *PLoS ONE* **13**, 1–22 (2019).

49. Gazeau, F. et al. Net ecosystem metabolism in a micro-tidal estuary (Randers Fjord, Denmark): evaluation of methods. *Mar. Ecol. Prog. Ser.* **301**, 23–41 (2005).

50. Medeiros, P. M., Sikes, E. L., Thomas, B. & Freeman, K. H. Flow discharge influences on input and transport of particulate and sedimentary organic carbon along a small temperate river. *Geochim. Cosmochim. Acta* **77**, 317–334 (2012).

51. Müller, D. et al. Fate of terrestrial organic carbon and associated CO_2 and CO emissions from two Southeast Asian estuaries. *Biogeosciences* **13**, 691–705 (2016).

52. Wiegner, T. N., Tubal, R. L. & MacKenzie, R. A. Bioavailability and export of dissolved organic matter from a tropical river during base- and stormflow conditions. *Limnol. Oceanogr.* **54**, 1233–1242 (2009).

53. Jiang, L. Q., Cai, W. & Wang, Y. A comparative study of carbon dioxide degassing in river- and marine-dominated estuaries. *Limnol. Oceanogr.* **53**, 2603–2615 (2008).

54. Alongi, D. M. Carbon cycling and storage in mangrove forests. *Ann. Rev. Mar. Sci.* **6**, 195–219 (2014).

55. Bouillon, S. et al. Mangrove production and carbon sinks: a revision of global budget estimates. *Global Biogeochem. Cycles* **22**, 1–12 (2008).

56. Ray, R., Baum, A., Rixen, T., Gleixner, G. & Jana, T. K. Exportation of dissolved (inorganic and organic) and particulate carbon from mangroves and its implication to the carbon budget in the Indian Sundarbans. *Sci. Total Environ.* **621**, 535–547 (2018).

57. Taillardat, P. et al. Carbon dynamics and inconstant porewater input in a mangrove tidal creek over contrasting seasons and tidal amplitudes. *Geochim. Cosmochim. Acta* **237**, 32–48 (2018).

58. Chen, X. et al. The mangrove CO2 pump: tidally driven pore-water exchange. *Limnol. Oceanogr.* **66**, 1563–1577 (2021).

59. Akhand, A. et al. Lateral carbon fluxes and CO_2 evasion from a subtropical mangrove-seagrass-coral continuum. *Sci. Total Environ.* **752**, 1–14 (2021).

60. Borges, A. V. et al. Atmospheric CO2 flux from mangrove surrounding waters. *Geophys. Res. Lett.* **30**, 12–15 (2003).

61. Abril, G. et al. Oxic/anoxic oscillations and organic carbon mineralization in an estuarine maximum turbidity zone (The Gironde, France). *Limnol. Oceanogr.* **44**, 1304–1315 (1999).

62. Abril, G. et al. A massive dissolved inorganic carbon release at spring tide in a highly turbid estuary. *Geophys. Res. Lett.* **31**, 2–5 (2004).

63. Crosswell, J. R., Carlin, G. & Steven, A. Controls on carbon, nutrient, and sediment cycling in a large, semiarid estuarine system; Princess Charlotte Bay, Australia. *J. Geophys. Res. Biogeosciences* **125**, 1–26 (2020).

64. Reithmaier, G. M. S., Ho, D. T., Johnston, S. G. & Maher, D. T. Mangroves as a source of greenhouse gases to the atmosphere and alkalinity and dissolved carbon to the coastal ocean: a case study from the Everglades National Park, Florida. *J. Geophys. Res. Biogeosciences* **125**, 1–16 (2020).

65. Polsenaere, P. et al. Seasonal, diurnal, and tidal variations of dissolved inorganic carbon and pCO_2 in surface waters of a temperate coastal lagoon (Arcachon, SW France). *Estuaries Coasts* **46**, 128–148 (2023).

66. Yang, W. Bin et al. Diurnal variation of CO2, CH4, and N2O emission fluxes continuously monitored in-situ in three environmental habitats in a subtropical estuarine wetland. *Mar. Pollut. Bull.* **119**, 289–298 (2017).

67. de la Paz, M., Gómez-Parra, A. & Forja, J. Inorganic carbon dynamic and air-water CO_2 exchange in the Guadalquivir Estuary (SW Iberian Peninsula). *J. Mar. Syst.* **68**, 265–277 (2007).

68. Ruiz-Halpern, S., Maher, D. T., Santos, I. R. & Eyre, B. D. High CO_2 evasion during floods in an Australian subtropical estuary downstream from a modified acidic floodplain wetland. *Limnol. Oceanogr.* **60**, 42–56 (2015).

69. Harley, J. F. et al. Spatial and seasonal fluxes of the greenhouse gases N_2O, CO_2 and CH_4 in a UK Macrotidal estuary. *Estuar. Coast. Shelf Sci.* **153**, 62–73 (2015).

70. Joesoef, A., Huang, W.-J., Gao, Y. & Cai, W. Air–water fluxes and sources of carbon dioxide in the Delaware Estuary: spatial and seasonal variability. *Biogeosciences* **12**, 6085–6101 (2015).

71. Creese, R. G., Glasby, T. M., West, G. & Gallen, C. Mapping the habitats of NSW estuaries. *Ind. Invest. NSW – Fish. Final Rep. Ser.* 1–90 (2009).

72. Williams, R. J., West, G., Morrison, D., Creese, R. G. Estuarine Resources of New South Wales, in: *Comprehensive Coastal Assessment. NSW Department of Primary Industries*, (Port Stephens, 2007).

73. Duarte, C. M. et al. Seagrass community metabolism: assessing the carbon sink capacity of seagrass meadows. *Global Biogeochem. Cycles* **24**, 1–8 (2010).

74. Maher, D. T. & Eyre, B. D. Benthic fluxes of dissolved organic carbon in three temperate Australian estuaries: Implications for global estimates of benthic DOC fluxes. *J. Geophys. Res. Biogeosciences* **115** (2010).

75. Bouillon, S. et al. Dynamics of organic and inorganic carbon across contiguous mangrove and seagrass systems (Gazi Bay, Kenya.). *J. Geophys. Res. Biogeosciences* **112**, 1–14 (2007). .

76. Eyre, B. D. & Ferguson, A. J. P. Comparison of carbon production and decomposition, benthic nutrient fluxes and denitrification in seagrass, phytoplankton, benthic microalgae- and macroalgae-dominated warm-temperate Australian lagoons. *Mar. Ecol. Prog. Ser* **229**, 43–59 (2002).

77. Koop, K., Bally, R. & McQuaid, C. D. The ecology of South African estuaries. Part XII: The Bot River, a closed estuary in the south-western Cape. *South African. J. Zool.* **18**, 1–10 (1983).

78. Roy, P. et al. Structure and Function of South-east Australian Estuaries. *Estuar. Coast. Shelf Sci.* **53**, 351–384 (2001).

79. Kuo, J. & McComb, A. J. in *Biology of Seagrasses: A Treatise on the Biology of Seagrasses with Special Reference to the Australian Region* (eds. Larkum, A. W. D., McComb, A. J. & Shepherd, S. A.) 6–73 (Elsevier, 1989).

80. Larkum, A. W. D. & den Hartog, C. in *Biology of Seagrasses: A Treatise on the Biology of Seagrasses with Special Reference to the Australian Region* (eds. Larkum, A. W. D., McComb, A. J. & Shepherd, S. A.) 112–156 (Elsevier, 1989).

81. Cresswell, I. D. & Semeniuk, V. in *Threats to Mangrove Forests* (eds. Makowksi, C. & Finkl, C.) 3–22 (Springer, 2018).

82. Matthews, J. B. & Matthews, J. B. R. Physics of climate change: harmonic and exponential processes from in situ ocean time series observations show rapid asymmetric warming. *J. Adv. Phys.* **6**, 1135–1171 (2014).

83. Bogard, M. J. et al. Hydrologic export is a major component of coastal wetland carbon budgets. *Global Biogeochem. Cycles* **34**, 1–14 (2020).

84. Eyre, B. D. Transport, retention and transformation of material in Australian estuaries. *Estuaries* **21**, 540–551 (1998).

85. McMahon, T. A. & Finlayson, B. L. Droughts and anti-droughts: the low flow hydrology of Australian rivers. *Freshw. Biol.* **48**, 1147–1160 (2003).

86. Borja, A. et al. in *Treatise on Estuarine and Coastal Science* (eds. Wolanski, E. & McLusky, D.) Vol. 1, 125–162 (Academic Press, 2012).

87. Maher, D. T. et al. Novel use of cavity ring-down spectroscopy to investigate aquatic carbon cycling from microbial to ecosystem scales. *Environ. Sci. Technol.* **47**, 12938–12945 (2013).

88. Pierrot, D. et al. Recommendations for autonomous underway pCO_2 measuring systems and data-reduction routines. *Deep. Res. II Top. Stud. Oceanogr.* **56**, 512–522 (2009).

89. Oakes, J. M., Eyre, B. D., Middelburg, J. J. & Boschker, H. T. S. Composition, production, and loss of carbohydrates in sub-tropical shallow subtidal sandy sediments: Rapid processing and long-term retention revealed by 13C-labeling. *Limnol. Oceanogr.* **55**, 2126–2138 (2010).

90. Dickson, A. G. Standards for ocean measurements. *Oceanography* **23**, 34–47 (2010).

91. Gafar, N. A. & Schulz, K. G. A three-dimensional niche comparison of Emiliania huxleyi and Gephyrocapsa oceanica: reconciling observations with projections. *Biogeosciences* **15**, 3541–3560 (2018).

92. Wetzel, R. G. & Likens, G. E. in *Limnological Analyses* 57–72 (Springer New York, 2000).

93. Climate Data Online. *Bureau of Meteorology, Commonwealth of Australia* http://www.bom.gov.au/climate/data/ (2019).

94. Wanninkhof, R. Relationship between wind speed and gas exchange over the ocean revisited. *Limnol. Oceanogr. Methods* **12**, 351–362 (2014).

95. Weiss, R. F. Carbon dioxide in water and seawater: the solubility of a non-ideal gas. *Mar. Chem.* **2**, 203–215 (1974).

96. Lan, X., Tans, P. & Thoning, K. W. Trends in globally-averaged CO_2 determined from NOAA Global Monitoring Laboratory measurements. https://doi.org/10.15138/9N0H-ZH07.

97. Rosentreter, J. A. et al. Spatial and temporal variability of CO_2 and CH_4 gas transfer velocities and quantification of the CH4 micro-bubble flux in mangrove dominated estuaries. *Limnol. Oceanogr.* **62**, 561–578 (2017).

98. Amorocho, J. & DeVries, J. J. A new evaluation of the wind stress coefficient over water surfaces. *J. Geophys. Res.* **85**, 433–442 (1980).

99. Abril, G., Commarieu, M. V., Sottolichio, A., Bretel, P. & Guérin, F. Turbidity limits gas exchange in a large macrotidal estuary. *Estuar. Coast. Shelf Sci.* **83**, 342–348 (2009).

100. McArdle, B. H. & Anderson, M. J. Variance heterogeneity, transformations, and models of species abundance: a cautionary tale. *Can. J. Fish. Aquat. Sci.* **61**, 1294–1302 (2004).

Author contributions
All authors have agreed to be listed and have approved the submitted version of the manuscript. JY conceived the project, collected data, ran data analysis and interpretation, and led the writing of the manuscript. JR and JO collected data, contributed to interpretation, and helped write the manuscript. BE conceived the project, collected data, contributed to interpretation, and helped write the manuscript. KS contributed to data analysis, and helped write the manuscript.

Competing interests
The authors declare no competing interests.

Additional information
Supplementary information The online version contains supplementary material available at https://doi.org/10.1038/s41467-024-48178-4.

Correspondence and requests for materials should be addressed to Jacob Z.-Q. Yeo.

Peer review information *Nature Communications* thanks the anonymous, reviewers for their contribution to the peer review of this work. A peer review file is available.

Reprints and permissions information is available at http://www.nature.com/reprints

Publisher's note Springer Nature remains neutral with regard to jurisdictional claims in published maps and institutional affiliations.